New Journal of Physics
The open-access journal for physics

Particle entrapment in a fluid suspension as a feedback effect

Sergey Shklyaev[1] **and Arthur V Straube**[2,3,4]

[1] Department of Theoretical Physics, Perm State University, Bukirev 15, 614990 Perm, Russia
[2] Institut für Theoretische Physik, Technische Universität Berlin, Hardenbergstrasse 36, D-10623 Berlin, Germany
[3] Department of Physics and Astronomy, University of Potsdam, Karl-Liebknecht-Strasse 24/25, D-14476 Potsdam-Golm, Germany
E-mail: arthur.straube@gmail.com

New Journal of Physics **10** (2008) 063030 (12pp)
Received 30 December 2007
Published 25 June 2008
Online at http://www.njp.org/
doi:10.1088/1367-2630/10/6/063030

Abstract. We consider a suspension of polarizable sub-micron particles under the action of a traveling wave dielectrophoresis (DEP). Our focus is specifically on particle-induced effects. When no external forces are exerted on the fluid and the particles are driven only by a DEP force, the joint motion of the particles can induce a steady fluid flow, leading to particle entrapment. The particle feedback effect is proven to be non-negligible even for a small volume concentration of particles.

[4] Author to whom any correspondence should be addressed.

Contents

1. Introduction

Particle dynamics in fluid flows has been the focus of attention for a long time, in various contexts and at different scales. These studies range from general problems of chaotic advection [1, 2], including passive [3, 4] and active [5] mass transfer in geophysical flows, to the problems of mixing [6] and the dynamics of complex fluids at microscales.

The fundamental aspects of particle dynamics in fluid flows at small scales are of great interest for numerous applications in medicine, biotechnology and pharmaceutical research [7]. The ability to manipulate particles is of particular importance for micro- and nanofluidics [8]. In these applications, the particles can be physical (colloids, liquid droplets in microemulsions, or small bubbles) or biological (cells, bacteria, or biopolymers) objects manipulated with electrokinetic [9, 10] or magnetic [11] forces, ultrasound [12], or optical tweezers [13].

Despite noticeable progress in understanding the impact of hydrodynamic [10, 14] and stochastic [15, 16] forces on the dynamics of the particles, the opposite problem of backward coupling, i.e. the influence of particle dynamics on the fluid, or *particle feedback*, is not fully understood. Especially challenging in the context of laminar flows is the problem of *integral* feedback effects, which are conventionally neglected. These effects are induced by a collection of *jointly* moving particles and can be non-negligible even for a small volume concentration of particles. A remarkable example is the particle entrapment under gravity first reported by Stommel [17], where the sedimenting under gravity particles are trapped by a macroscopic vortex flow. A long-living cloud formed by the trapped particles stays suspended for a very long time. As has been recently demonstrated [18], the particle feedback for such system results in a very strong suppression of the carrier vortex flow.

Further efforts in understanding particle entrapment involve problems such as the impact of particle inertia [19], non-spherical form of particles [20] and additional non-uniform forces [21]. Small inertia makes the cloud of heavy trapped particles unstable, whereas for light particles accumulation effects take place [19]. The particle non-sphericity changes the form of the trapped cloud [20] and an additional dielectrophoretic (DEP) force allows to control the entrapment process, which is combined with accumulation effects [21].

In the present paper, we systematically address the general problem of particle feedback at small scales, where diffusion of particles becomes non-negligible. In contrast to the entrapment in macroscopic flows [17]–[20], we focus on the situation where the classical Stommel mechanism of entrapment is no longer efficient, as the cloud of trapped particles is rather quickly smeared out by diffusion. Moreover, all these previous studies including [21] are based on the existence of a vortex flow. This flow is a necessary ingredient for entrapment and it exists irrespective of the particles. What is important in our study is that such vortex flow is induced by the particles and cannot arise otherwise. We introduce an original theoretical model and apply it to a physically realistic problem. We predict a novel mechanism of particle entrapment, which is not only fundamentally different from the one conventionally known [17, 19, 21] but also is proven to be efficient at small scales.

2. Theoretical model

2.1. General approach allowing for particle feedback

We start by formulating a continuum model for spherical noninteracting particles of radius a suspended in a fluid having viscosity η and density ρ. To focus only on feedback effects, we impose a nonuniform external force $\bar{\mathbf{F}}(\bar{\mathbf{r}})$ on the particles, which does not directly influence the carrier phase. Hereafter, the bars are used to denote the dimensional variables. If both the size of the particles relative to the length scale L of the flow (a/L) and the volume fraction of particles $\bar{\varphi}$ are small, a model allowing for the feedback describes the dynamics of the two-phase system:

$$\rho\left(\frac{\partial\bar{\mathbf{u}}}{\partial\bar{t}}+\bar{\mathbf{u}}\cdot\bar{\nabla}\bar{\mathbf{u}}\right)=-\bar{\nabla}\bar{p}+\eta\bar{\nabla}^2\bar{\mathbf{u}}+\bar{\varphi}\bar{\mathbf{F}}, \tag{1}$$

$$\bar{\nabla}\cdot\bar{\mathbf{u}}=0, \quad \bar{\mathbf{v}}=\bar{\mathbf{u}}+\frac{2a^2}{9\eta}\bar{\mathbf{F}}, \tag{2}$$

$$\frac{\partial\bar{\varphi}}{\partial\bar{t}}+\bar{\nabla}\cdot\bar{\mathbf{j}}=0, \quad \bar{\mathbf{j}}=\bar{\varphi}\bar{\mathbf{v}}-D\bar{\nabla}\bar{\varphi}, \tag{3}$$

where $\bar{\mathbf{u}}$ and $\bar{\mathbf{v}}$ are the fluid and particle velocities, respectively, $\bar{p}$ is the pressure, $\bar{\varphi}$ is the volume fraction of particles, $\bar{\mathbf{j}}$ is the particle flux and D is the diffusivity of particles.

The proposed model (1)–(3) is a natural generalization of the theory developed in [18]. Compared to the previous analysis valid for a constant external force, we now allow for an arbitrary spatially dependent $\bar{\mathbf{F}}(\bar{\mathbf{r}})$. Another distinction that significantly changes the physics behind the entrapment effect is taking into consideration the diffusion of particles. The corresponding contribution now enters the particle flux $\bar{\mathbf{j}}$ in equation (3). On the other hand, in the partial case of $\bar{\mathbf{u}}=0$ our model is in agreement with the study [10] and correctly reproduces the known results. Here, the model (1)–(3) is reduced to the equation that describes a mechanical equilibrium distribution of polarizable particles under DEP force, see section 3.2.

Of special emphasis is taking into consideration the particle feedback. In contrast to [18], in our study only the particles are able to cause the fluid to move, which is an advantageous feature because the fluid flow itself becomes a perfect indicator for the particle feedback. The feedback is described by the last term in the Navier–Stokes equation, see equation (1). Physically, this term originates from the Stokes drag, $\gamma\bar{\varphi}(\bar{\mathbf{v}}-\bar{\mathbf{u}})$, where $\gamma=9\eta/2a^2$. For small a/L, this

contribution dominates in the interphase force [19, 22] and is balanced by $\bar{\mathbf{F}}$. At the same time, this type of balance results in a distinction between the velocities of the two phases, where inertia corrections are negligible, see the second relation equation (2). As a result, the feedback term turns out to be proportional to $\bar{\varphi}$ and $\bar{\mathbf{F}}$, which reflects an intuitively clear expectation. The particle feedback effects are more pronounced for a bigger number of particles and higher intensity of the external force. Note, that a very similar approach has been recently applied to describe the dynamics of magnetized ferrofluids in magnetic fields [23] and suspensions under vibrations [24].

Let us now formulate our model (1)–(3) in terms of dimensionless variables. First, by presenting the volume fraction of particles and the external force as $\bar{\varphi} = \Phi_0\varphi$ and $\bar{\mathbf{F}} = F_0\mathbf{F}$, we introduce their reference values Φ_0 and F_0, respectively. Here, the factor Φ_0, which can be thought of as the space-averaged volume fraction of particles, ensures the smallness of $\bar{\varphi}$ so that the rescaled field φ takes *finite* values. The value of F_0 and the dimensionless field $\mathbf{F}$ are problem dependent, we specify them later, in section 3. Next, we use the scales of L, L^2/D, D/L, $\eta D/L^2$ and Φ_0 for the length, time, velocity, pressure and particle volume fraction, respectively. As a result, we arrive at the dimensionless equations

$$\frac{1}{\mathrm{Sc}}\left(\frac{\partial \mathbf{u}}{\partial t} + \mathbf{u}\cdot\nabla\mathbf{u}\right) = -\nabla p + \nabla^2\mathbf{u} + Q_\mathrm{s}\langle\Phi\rangle\varphi\mathbf{F}, \tag{4}$$

$$\nabla\cdot\mathbf{u} = 0, \quad \mathbf{v} = \mathbf{u} + Q_\mathrm{s}\mathbf{F}, \tag{5}$$

$$\frac{\partial\varphi}{\partial t} + \nabla\cdot\mathbf{j} = 0, \quad \mathbf{j} = \varphi\mathbf{v} - \nabla\varphi. \tag{6}$$

Here, $Q_\mathrm{s} = 2a^2LF_0/9\eta D$ represents the intensity of the external field, $\mathrm{Sc} = \eta/D\rho$ is the Schmidt number, and a ratio of two asymptotically small parameters $\langle\Phi\rangle = 9L^2\Phi_0/2a^2$ is the feedback parameter, which is assumed to be finite.

To stress the relevance of our approach, we provide estimations for a realistic system. We use parameters, which are relatively close to the specific setup data [10, 25, 26]. For a water ($\eta \simeq 10^{-2}\,\mathrm{g\,cm^{-1}\,s^{-1}}$, $\rho \simeq 1.0\,\mathrm{g\,cm^{-3}}$) suspension with particle size $a \simeq 200\,\mathrm{nm}$ and $\Phi_0 \simeq 3\%$ in a container of a characteristic size $2L \simeq 25\,\mu\mathrm{m}$ at 300 K one obtains $\langle\Phi\rangle \simeq 500$, and, according to Einstein's formula, $D \simeq 10^{-8}\,\mathrm{cm^2\,s^{-1}}$ and $\mathrm{Sc} \simeq 10^6$. Although in most conventional situations $\mathrm{Sc} \gg 1$, it becomes necessary to account for the diffusion of particles. The reason is twofold: (i) even small diffusion becomes non-negligible at small scales, e.g. when the diffusion time is of the order of $L^2/D \simeq 100\,\mathrm{s}$ and (ii) it prevents from unbounded accumulation of particles by the external field. For a wide range of dielectric fluids, the situation which is also addressed next, the densities and viscosities are close to those of water. For instance, for carbon tetrachloride (CCl_4) $\rho \simeq 1.59\,\mathrm{g\,cm^{-3}}$, $\eta \simeq 0.73\times10^{-2}\,\mathrm{g\,cm^{-1}\,s^{-1}}$ and for a hydrocarbon liquid such as decane we have $\rho \simeq 0.73\,\mathrm{g\,cm^{-3}}$, $\eta \simeq 0.92\times10^{-2}\,\mathrm{g\,cm^{-1}\,s^{-1}}$. Thus, the arguments and estimations provided remain perfectly valid for these organic fluids.

2.2. DEP force

We now focus on an example of a DEP force exerted on polarizable particles under an ac electric field $\mathbf{E}(\mathbf{r}, t) = \mathrm{Re}[\tilde{\mathbf{E}}(\mathbf{r})\exp(\mathrm{i}\omega t)]$. Hereafter, ω is the angular frequency, $\mathrm{Re}[z] \equiv z_\mathrm{r}$ and

$\mathrm{Im}[z] \equiv z_\mathrm{i}$ denote the real and imaginary parts of z. The time-averaged force (per unit volume) is [10, 27]

$$\bar{\mathbf{F}} = \tfrac{3}{2}\epsilon_\mathrm{m}\mathrm{Re}\left[\tilde{K}(\omega)\tilde{\mathbf{E}}\cdot\bar{\nabla}\tilde{\mathbf{E}}^*\right], \tag{7}$$

where '*' indicates the complex conjugate. The complex frequency-dependent function $\tilde{K}(\omega) = (\tilde{\epsilon}_\mathrm{p} - \tilde{\epsilon}_\mathrm{m})/(\tilde{\epsilon}_\mathrm{p} + 2\tilde{\epsilon}_\mathrm{m})$ is a measure of the effective polarizability of the particle, known as the Clausius–Mossotti factor. Here, $\tilde{\epsilon}_\mathrm{p}$ and $\tilde{\epsilon}_\mathrm{m}$ are the complex permittivities of the particles and the fluid medium, respectively. The complex permittivity is defined as $\tilde{\epsilon} = \epsilon - \mathrm{i}\sigma/\omega$ (where ϵ is the permittivity and σ is the conductivity of the medium). The DEP force (7) comprises two independent contributions:

$$\bar{\mathbf{F}} = \frac{3}{4}\epsilon_\mathrm{m}\tilde{K}_\mathrm{r}\,\bar{\nabla}|\tilde{\mathbf{E}}|^2 - \frac{3}{2}\epsilon_\mathrm{m}\tilde{K}_\mathrm{i}\,\bar{\nabla}\times\left(\tilde{\mathbf{E}}_\mathrm{r}\times\tilde{\mathbf{E}}_\mathrm{i}\right). \tag{8}$$

The first term relates to the in-phase component of the induced dipole. This force points toward the domains of higher field strength for $\tilde{K}_\mathrm{r} > 0$ or, conversely, toward the domains of weaker fields for $\tilde{K}_\mathrm{r} < 0$, which is referred to as *positive*-DEP (*p*-DEP) or *negative*-DEP (*n*-DEP), respectively [28]. Accordingly, the particles are either attracted or repelled by the electrodes. The second term arises owing to the out-of-phase component of the dipole and is nonvanishing if the phase is spatially varying [29, 30], e.g. for traveling wave DEP. This term causes the particles to move parallel to the electrodes.

It is necessary to ensure that the feedback effects are not hindered by other possible sources of fluid motion. Applied electric fields induce temperature gradients through Joule heating and therefore create nonuniformities in the conductivity, permittivity and density in the fluid, which can lead to electroconvection and/or natural convection [10]. The temperature differences produced by the electric field in the fluid is $\delta\bar{T} \sim \sigma_\mathrm{m}U_0^2\kappa^{-1}$ and the typical electrothermal force on the fluid can be evaluated as [10, 25]:

$$\bar{F}_\mathrm{ET} \sim \epsilon_\mathrm{m}\frac{U_0^2}{L^3}\delta\bar{T}\max\left(\beta_\epsilon, \beta_\sigma\right), \quad \beta_\epsilon = \frac{1}{\epsilon_\mathrm{m}}\frac{\mathrm{d}\epsilon_\mathrm{m}}{\mathrm{d}\bar{T}}, \quad \beta_\sigma = \frac{1}{\sigma_\mathrm{m}}\frac{\mathrm{d}\sigma_\mathrm{m}}{\mathrm{d}\bar{T}}, \tag{9}$$

where κ is the thermal diffusivity of the liquid and U_0 is a characteristic value of the electric potential. This force is negligible compared to the feedback term in equation (4) $\bar{F}_\mathrm{fb} \equiv \Phi_0 F_0 \sim \epsilon_\mathrm{m}\Phi_0 U_0^2 L^{-3}$ (see equation (7)), provided that

$$\frac{\bar{F}_\mathrm{ET}}{\bar{F}_\mathrm{fb}} \sim \frac{\sigma_\mathrm{m}U_0^2}{\kappa\Phi_0}\max\left(\beta_\epsilon, \beta_\sigma\right) \ll 1 \tag{10}$$

is satisfied. To guarantee predominance of the feedback effects we restrict our analysis by consideration of dielectric fluids. For instance, for decane with $\sigma_\mathrm{m} \simeq 10^{-12}\,\mathrm{S\,m^{-1}}$, $\beta_\sigma < \beta_\epsilon \simeq 0.6\times10^{-3}\,\mathrm{K^{-1}}$, $\kappa \simeq 0.15\,\mathrm{Wm^{-1}K^{-1}}$ and for $U_0 \simeq 2\,\mathrm{V}$ we obtain a value for $\bar{F}_\mathrm{ET}/\bar{F}_\mathrm{fb}$ of the order of 10^{-12}. For carbon tetrachloride the estimation results in an order of magnitude higher ratio. Moreover, even for deionized water ($\sigma_\mathrm{m} \simeq 2\,\mu\mathrm{S\,cm^{-1}}$, $\beta_\sigma \simeq 0.02\,\mathrm{K^{-1}}$, $\beta_\epsilon \simeq -0.004\,\mathrm{K^{-1}}$, $\kappa \simeq 0.58\,\mathrm{Wm^{-1}\,K^{-1}}$) as applied in [21], and for $U_0 \simeq 0.3\,\mathrm{V}$, which corresponds to desirable values of Q_s (see section 3), we obtain a value for $\bar{F}_\mathrm{ET}/\bar{F}_\mathrm{fb}$ of the order of 5×10^{-5}. These estimations clearly indicate the prevalence of particle feedback over the thermal effects, which is valid not only for dielectric fluids.

Next, as we claim below, weaker voltage is enough to cause the feedback-induced flow (as compared with conventionally applied $U_0 \simeq 5$–$10\,\mathrm{V}$ in [10, 21, 26]). Although the low conductivity assumption is of no principal significance, it simplifies the forthcoming analysis.

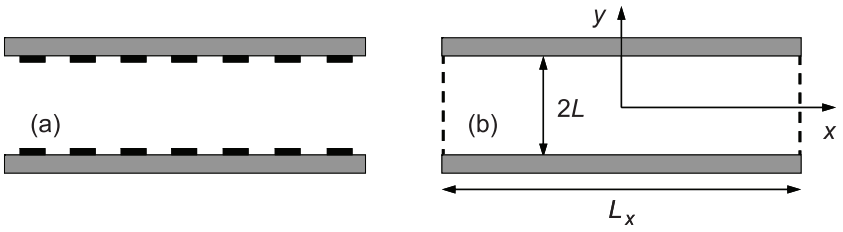

Figure 1. Problem geometry. A sketch of a typical experimental setup on traveling wave DEP (a) with electrode arrays (in black), see, e.g. [10, 26]. The simplified geometry used in our theoretical study (b).

Within this approximation, natural convection and ac electro-osmosis are even weaker effects than electroconvection and therefore can be neglected as well.

3. Traveling-wave DEP in a rectangular container

3.1. Problem statement

We now turn to the analysis of a typical system for experiments on traveling wave DEP [10, 26]. To focus solely on the mechanism of particle feedback, in this study we perform a simplified analysis. As has been justified before, see, e.g. [9, 31], we ignore the electrode micro-structure (see figure 1) and approximate the traveling wave by a one-harmonic signal. Thus, we consider a two-phase medium filling a rectangular container of sides L_x, $L_y \equiv 2L$, L_z and impose a traveling electric-potential wave at the boundaries $\bar{y} = \pm L : \bar{\phi} = U_0 \exp[\mathrm{i}(\omega\bar{t} - q\bar{x})]$, where q is the wave number and U_0 is the amplitude. The complex amplitude $\tilde{\phi}(\bar{\mathbf{r}})$ (where $\tilde{\mathbf{E}} = -\bar{\nabla}\tilde{\phi}$) obeys the Laplace equation, $\bar{\nabla}^2\tilde{\phi} = 0$, which is readily solved. Assuming that $L_y \ll L_x$, $L_y \ll L_z$ and that the sidewalls are electrically passive, we obtain $\tilde{\phi}(\bar{\mathbf{r}}) = U_0 \exp(-\mathrm{i}q\bar{x})(\cosh q\bar{y})/\cosh qL$ and evaluate

$$\mathbf{F}(\mathbf{r}) = (-K_\mathrm{i} \cosh by,\ \sinh by,\ 0). \tag{11}$$

Here, we define $F_0 = 3\epsilon_\mathrm{m} U_0^2 q^3 \tilde{K}_\mathrm{r}/2\cosh^2(b/2)$ and introduce a dimensionless parameter $K_\mathrm{i} = \tilde{K}_\mathrm{i}/\tilde{K}_\mathrm{r}$ and the dimensionless wavenumber $b = 2qL$. A traveling wave of period 50 μm leads to $b \approx 3$ and $|Q_\mathrm{s}| \approx 0.37$ for decane and $|Q_\mathrm{s}| \approx 0.29$ for deionized water (these estimations are based on the specific setup data as used before). Next, we restrict our consideration to the case of $K_\mathrm{i} > 0$, which holds for any dielectric fluid. This restriction is made for the sake of simplicity and is not principal because for a conductive fluid the sign reversal of K_i changes only the direction of the induced flow.

3.2. Mechanical equilibrium

We first point out the partial case of $K_\mathrm{i} = 0$, which corresponds to the limit of perfectly dielectric particles. According to (11), there is no force allowing for particle transport along the plane boundaries $y = \pm 1$, thus, only transversal redistribution occurs. The particles tend to migrate either toward or away from these boundaries, which is counterbalanced by diffusion; longitudinal nonuniformities are smeared by diffusion. Thus, the case $K_\mathrm{i} = 0$ admits a state of

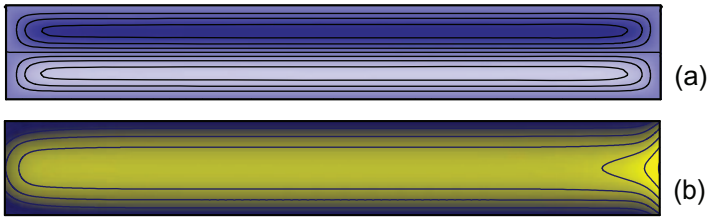

Figure 2. Contourplots of the streamfunction (a) and particle concentration (b) in the steady state for $\mathrm{Sc} = 2$, $Q_\mathrm{s} = -0.2$, $K_\mathrm{i} = 1$, $b = 3$ and $\langle\Phi\rangle = 575$. Lighter (clockwise rotation for vortices) and darker (counterclockwise rotation) colored domains refer to higher and lower values of the plotted fields, respectively. The distribution of particles away from the sidewalls corresponds to solution (12), the maximum of the concentration close to the sidewalls is up to 10% higher than away from them.

mechanical equilibrium described by the quiescent fluid $\mathbf{u}_0(\mathbf{r}) = 0$, a vanishing particle flux $\mathbf{j}_0(\mathbf{r}) = 0$, and a nonuniform distribution of particles

$$\varphi_0(\mathbf{r}) = C_0\Psi_0(y), \qquad \Psi_0(y) = \exp\left(Q_\mathrm{s} b^{-1}\cosh by\right), \tag{12}$$

where $C_0 = [\int_0^1 \Psi_0(y)\,\mathrm{d}y]^{-1}$, as by definition the averaged φ is unity. The concentration profile (12) describes the accumulation of particles near the boundaries for $Q_\mathrm{s} > 0$, or in the center plane for $Q_\mathrm{s} < 0$, which correspond to *p*-DEP or *n*-DEP, respectively. The solution (12) is in agreement with the concentration profile obtained in [10]. Analytical and numerical treatment of the linearized problem as well as a direct numerical simulation of the nonlinear model (4)–(6) with (11) indicate that the state of mechanical equilibrium is stable for any values of the governing parameters.

3.3. Mechanical non-equilibrium state: particle entrapment

What happens in a more general case of conductive particles in which $K_\mathrm{i} \neq 0$ and longitudinal transport is allowed, is a simple question to pose, but is remarkably difficult to answer. In the limiting case of no feedback, i.e. where $\langle\Phi\rangle \ll 1$, there is no source for fluid motion and the problem is reduced to finding a distribution $\varphi_0(\mathbf{r}) = \varphi_0(x, y)$ as governed by equations (5) and (6) with $\mathbf{u}(\mathbf{r}) = 0$. In the presence of the feedback, the problem becomes highly nontrivial, because the system is no longer in mechanical equilibrium. To get an impression of possible scenarios, we have numerically integrated equations (4)–(6) with (11) in a two-dimensional rectangular box with the no-slip condition for $\mathbf{u}$ and a vanishing normal component for $\mathbf{j}$ at the solid walls. A typical steady-state solution for a fixed value of Sc is presented in figure 2. Steady states corresponding to different Sc values are similar in appearance: a slight distinction comes from the nonlinear term, which is nonvanishing only near the sidewalls. What is general is that the flow is large-scaled and closed. The particles are involved in vortical motion, reminiscent of particle entrapment under gravity, which was first shown by Stommel [17] (see also [18]–[21]).

However, there are two principal differences to the previous studies. First and most important, the conventional entrapment implies the existence of a vortex flow irrespective of whether there are any particles or not [17]–[21]. The fluid flow in our system can be induced only by the particles. In contrast to previous studies, particle entrapment arises as a generic particle feedback effect, which also provides a way to generate a flow. The second important

distinction is that we carefully account for the effects of diffusion. These nontrivial diffusion effects have been systematically addressed neither in studies performed in a pure Hamiltonian framework [17, 18], nor in a non-Hamiltonian studies [19, 21].

A closer inspection of figure 2 shows that the flow and concentration patterns are one-dimensional everywhere except for in the vicinity of the sidewalls. This situation allows for a one-dimensional analysis of equations (4)–(6) with (11) away from the sidewalls, which is valid for systems with a high aspect ratio. Accordingly, we apply the ansatz $\varphi_0(\mathbf{r}) = \varphi_0(y)$, $\mathbf{u}_0(\mathbf{r}) = (u_0(y), 0, 0)$. Because the flow does not influence the distribution of particles, $\varphi_0(y)$ is given by formula (12) with the same C_0. To determine the fluid velocity, we account for the no-slip conditions at the solid walls $u_0(\pm 1) = 0$ and a condition of no mean fluid flux $\int_{-1}^{1} u_0 \, \mathrm{d}y = 0$, which implies that the flow is closed. As a result, we obtain:

$$u_0(y) = \alpha V_0(y), \quad V_0(y) = V_{01}(y) + V_{02}(y), \tag{13}$$

$$V_{01}(y) = I_2(1) - I_2(y), \quad V_{02}(y) = -\beta(1 - y^2), \tag{14}$$

where $\alpha = C_0\langle\Phi\rangle|Q_s K_i| > 0$, $\beta = 3[I_2(1) - I_3(1)]/2 > 0$, $I_1(y) = \int_0^y \Psi_0(\xi)\cosh b\xi \, \mathrm{d}\xi$ and $I_{l+1}(y) = \int_0^y I_l(\xi)\, \mathrm{d}\xi$ $(l = 1, 2)$; because of symmetry, $V_0(y)$ is an even function. Next, we impose the condition of particle entrapment $\int_{-1}^{1} \mathbf{j}_0 \cdot \mathbf{e}_x \, \mathrm{d}y = 0$ and $\mathbf{e}_x = (1, 0, 0)$, which ensures no mean particle flux [18]. We arrive at

$$\langle\Phi\rangle = I_1(1)\left(C_0 \int_0^1 V_0 \Psi_0 \, \mathrm{d}y\right)^{-1} \equiv \langle\Phi\rangle_c, \tag{15}$$

which represents a formal restriction on $\langle\Phi\rangle$. For every set of governing parameters, only a specific number of particles defined by (15) can be trapped by the flow. In practice, however, e.g. for a closed rectangular box, such a restriction is not stringent. For $\langle\Phi\rangle$ different from $\langle\Phi\rangle_c$, the solution away from the sidewalls still corresponds to (12), as $\langle\Phi\rangle = \langle\Phi\rangle_c$. Their actual distinction is balanced in the vicinities of the sidewalls, where a lack or excess of particles emerges, leading to local gradients of concentration on top of (12). This is clearly seen in figure 2(b), where for the chosen set of parameters $\langle\Phi\rangle_c = 442$. In most of the domain the solution is one-dimensional and corresponds to the entrapped state (12) with $\langle\Phi\rangle = \langle\Phi\rangle_c$. The noticeable distinction between $\langle\Phi\rangle = 575$ and $\langle\Phi\rangle_c$ has led to a local redistribution of particles: a relatively smaller lack of particles near the left wall and a larger excess near the right wall.

Of special attention is the case in which $\langle\Phi\rangle$ is considerably smaller than $\langle\Phi\rangle_c$. Here, although there are not enough particles to excite a flow in the whole domain, entrapment still occurs. As before, it is accompanied by the birth of a steady vortex flow, but of a smaller longitudinal extension. With the decrease of $\langle\Phi\rangle$, the vortices gradually shrink and no longer exist at the limit $\langle\Phi\rangle \ll 1$.

The characteristics of the one-dimensional state (12)–(15) are presented in figure 3. The particles tend to move along the x-axis; faster near the boundaries and slower at the center of the channel (see equations (5) and (11)). Because of viscous drag, the fluid is towed by the particles, which has two consequences. Firstly, this motion contributes in a positive fluid flux, defined by $V_{01}(y)$. Secondly, it creates a longitudinal gradient of pressure that gives rise to an opposite Poiseuille flow $V_{02}(y)$, with a maximal velocity at $y = 0$. The velocity profile $V_0(y)$ is a superposition of these counterflows, such that the net fluid flux is vanishing. It is worth noting that profile (13) qualitatively resembles the one in the convective flow in a vertical slot induced by internal sources of heat [32]. In our case, the role of the heat sources is played by

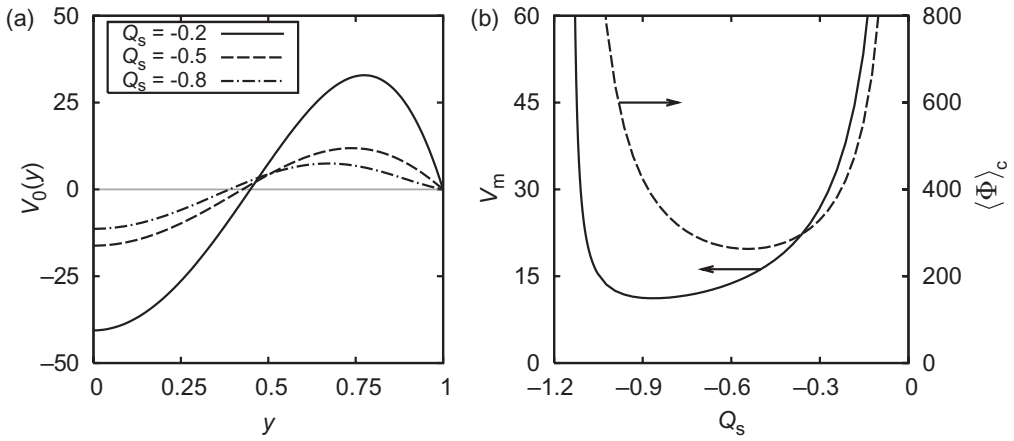

Figure 3. Characteristics of the one-dimensional state of entrapment (12)–(15) for $b = 3$: velocity profiles (a), maximal absolute velocity $V_m = \max_y |V_0(y)|$ and $\langle\Phi\rangle_c$ as functions of Q_s (b).

the nonuniform distribution of particles and the DEP force instead of gravity. Note that the state of entrapment exists only for $Q_c < Q_s < 0$, see figure 3(b). Beyond this range, equation (15) prescribes negative values of $\langle\Phi\rangle_c$, which is physically irrelevant. In particular, the condition $Q_s < 0$ manifests that the entrapment can be observed only for *n*-DEP. From the experimental point of view, the flow can be easily controlled by tuning the frequency of the imposed traveling wave. We also indicate that for $|Q_s| < |Q_c| \approx 1.2$ and $b \leqslant 3$ the particle distribution possesses no steep gradients, which directly follows from equation (12). The maximal value of the concentration $\varphi_m = \max(\varphi_0)$ is not large: $\varphi_m < 2$. For a sharper distribution of particles no entrapped state is possible.

3.4. Stability of the entrapped state

To explore the stability of the solution (12) and (13), we have introduced perturbations of the form $f(\mathbf{r}) = \hat{f}(y)\exp(\lambda t - ik_x x - ik_z z)$ and linearized equations (4)–(6) near this solution. Here $\lambda = \lambda_r + i\lambda_i$ is the complex growth rate, k_x and k_z are the wave numbers along the x- and z-axes. The analysis has shown that the modes with the largest λ_r correspond to the perturbations in the form of rolls, $k_z = 0$. We have checked a wide range of Schmidt numbers, the stability maps are presented in figure 4. The regions of stability and instability are separated by two curves $K_i^{(c)}(Q_s)$ of neutral behavior, for which $\lambda_r = 0$ (see figure 4(a)). These lines refer to a pair of competing modes of the largest λ_r and have different asymptotes for $\mathrm{Sc} \gg 1$.

For the branch with higher $|Q_s|$ the scaling law is $K_i^{(c)} = K_1\sqrt{\mathrm{Sc}}$. The concentration perturbations are localized close to the center plane $y = 0$. For the branch with lower $|Q_s|$, we have the asymptotics $K_i^{(c)} = K_2\,\mathrm{Sc}$. Here, the concentration perturbations are maximal in vicinities of the critical points where the particle velocity equals the phase velocity of the perturbations. A boundary layer arises near these critical points and even small diffusivity must be taken into account without compromise. This situation is akin to the well-known problem concerning the stability of the Poiseuille flow at large values of the Reynolds number [33], where the role of diffusivity is played by viscosity. As clarified by Lin, small viscosity cannot be neglected near the critical points, in which the flow velocity coincides with the phase velocity of perturbations.

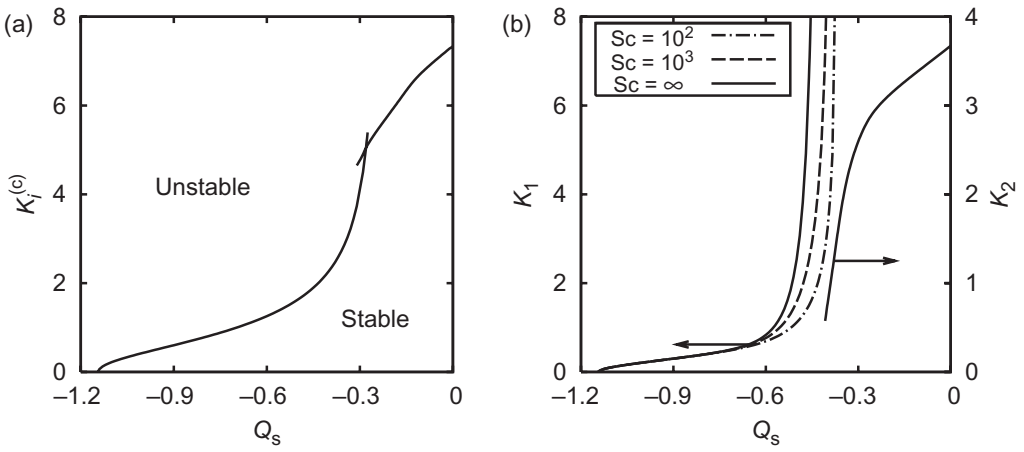

Figure 4. Stability maps for $b = 3$. Neutral stability curves for $\mathrm{Sc} = 2$ (a). Scaling functions $K_1(Q_s)$ and $K_2(Q_s)$ for different values of Sc (b).

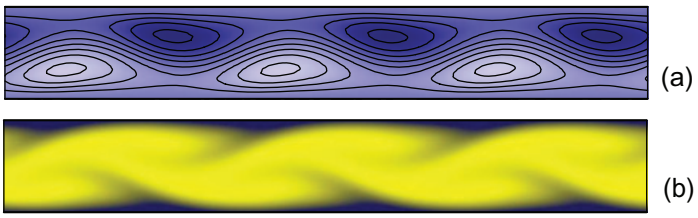

Figure 5. Breakdown of the one-dimensional state beyond the stability threshold, $\mathrm{Sc} = 2$, $Q_s = -0.2$, $K_i = 7$, $b = 3$, $\langle\Phi\rangle = 450$: streamfunction (a) and particle concentration (b). The coloring scheme is as in figure 2.

The dependencies $K_i^{(c)}\mathrm{Sc}^{-1/2}$ and $K_i^{(c)}\mathrm{Sc}^{-1}$ for different values of Sc are plotted in figure 4(b). With the growth of Sc, these dependencies converge to master curves $K_1(Q_s)$ and $K_2(Q_s)$. Because of the different scaling, the convergence of $K_i^{(c)}/\sqrt{\mathrm{Sc}}$ to K_1 is slower whereas the master curve K_2 is approached already at $\mathrm{Sc} = 100$.

The results of the linear stability analysis were confirmed by numerical integration of the nonlinear model (4)–(6) with (11). Note that for large values of Sc, the value $K_i^{(c)}$ is high and the instability in this particular situation is difficult to achieve experimentally. Indeed, high K_i means that $\tilde{K}_r \to 0$ and hence $Q_s \to 0$. As we see from both figure 3(b) and formula (13), the intensity of the one-dimensional flow becomes very high. However, instability can be found for moderate Sc. We have studied the breakdown of the one-dimensional state, which is found to occur supercritically. The patterns beyond the threshold (see figure 5 for a snapshot) travel along the x-axis with a speed of λ_i/k_x. For the different branches, the patterns look similar, but have distinct spatial periods and travel in opposite directions.

4. Conclusions

In conclusion, we have studied the role of the particle feedback in a two-phase system under the action of a traveling wave DEP. In a situation in which the particles are driven by the DEP

force but where no external forces are exerted on the fluid, the joint motion of the particles can induce a steady fluid flow, which is accompanied by a novel particle entrapment. In contrast to the conventional mechanism, diffusion of the particles becomes a necessary ingredient of the entrapment. This particle feedback effect has been proven to be non-negligible even for small volume concentration of particles. We note that similar phenomena are expected in various physical systems. Indeed, the set of equations (4)–(6) with a force in the form of equation (7) describe a wide class of problems, e.g. magnetized ferrofluids [23], particles driven by optical tweezers [13] and bubbly fluids under vibration [24], where the field $\tilde{\mathbf{E}}$ entering (7) is of a different nature.

Acknowledgments

We acknowledge fruitful discussions with S Hardt, A A Nepomnyashchy, A Pikovsky, B L Smorodin, V Steinberg and C Pooley. S S thanks DAAD and the Foundation 'Perm Hydrodynamics' for support; A S was supported by the German Science Foundation (DFG SPP 1164 'Nano- and microfluidics,' Project STR 1021/1).

References

[1] Aref H 1984 *J. Fluid Mech.* **143** 1
[2] Aref H 2002 *Phys. Fluids* **14** 1315
[3] Wiggins S 2005 *Annu. Rev. Fluid Mech.* **37** 295
[4] Koshel K V and Prants S V 2006 *Usp. Fiz. Nauk* **49** 1151
[5] Tél T, de Moura A, Grebogi C and Károlyi G 2005 *Phys. Rep.* **413** 91
[6] Ottino J M 1989 *The Kinematics of Mixing: Stretching, Chaos, and Transport* (Cambridge: Cambridge University Press)
[7] Whitesides G M 2006 *Nature* **442** 368
[8] Squires T M and Quake S R 2005 *Rev. Mod. Phys.* **77** 977
[9] Schnelle T, Müller T and Fuhr G 1999 *BioMethods* **10** 417
[10] Morgan H and Green N G 2003 *AC Electrokinetics: Colloids and Nanoparticles* (Baldock: Research Studies Press)
[11] Gijs M A M 2004 *Microfluidics Nanofluidics* **1** 22
[12] Hawkes J J, Cefai J J, Barrow D A, Coakley W T and Briarty L G 1998 *J. Phys. D: Appl. Phys.* **31** 1673
[13] Grier D G 2003 *Nature* **424** 810
[14] Kim S and Karrila S J 1991 *Microhydrodynamics: Principles and Selected Applications* (Boston: Butterworth-Heinemann)
[15] Reimann P 2002 *Phys. Rep.* **361** 57
[16] Reimann P and Hänggi P 2002 *Appl. Phys.* A **75** 169
[17] Stommel H 1949 *J. Mar. Res.* **8** 24
[18] Lyubimov D V, Straube A V and Lyubimova T P 2005 *Phys. Fluids* **17** 063302
[19] Maxey M R 1991 *Phil. Trans. R. Soc. Lond.* A **333** 289
[20] Mallier R and Maxey M 1991 *Phys. Fluids* A **3** 1481
[21] Tuval I, Mezić I, Bottausci F, Zhang Y T, MacDonald N C and Piro O 2005 *Phys. Rev. Lett.* **95** 236002
[22] Druzhinin O A 1995 *J. Fluid Mech.* **297** 49
[23] Shliomis M I and Smorodin B L 2002 *J. Magn. Magn. Mater.* **252** 197
[24] Straube A V, Lyubimov D V and Shklyaev S V 2006 *Phys. Fluids* **18** 053303
[25] Ramos A, Morgan H, Green N G and Castellanos A 1998 *J. Phys. D: Appl. Phys.* **31** 2338
[26] Felten M, Geggier P, Jäger M and Duschl C 2006 *Phys. Fluids* **18** 051707

[27] Green N G, Ramos A and Morgan H 2000 *J. Phys. D: Appl. Phys.* **33** 632
[28] Pohl H A 1978 *Dielectrophoresis* (Cambridge: Cambridge University Press)
[29] Hagedorn R, Fuhr G, Müller T and Gimsa J 1992 *Electrophoresis* **13** 49
[30] Wang X-B, Huang Y, Becker F F and Gascoyne P R C 1994 *J. Phys. D: Appl. Phys.* **27** 1571
[31] Fuhr G, Schnelle T and Wagner B 1994 *J. Micromech. Microeng.* **4** 217
[32] Gershuni G Z and Zhukhovitsky E M 1976 *Convective Stability of Incompressible Fluid* (Jerusalem: Keter)
[33] Lin C C 1955 *The Theory of Hydrodynamic Stability* (Cambridge: Cambridge University Press)